

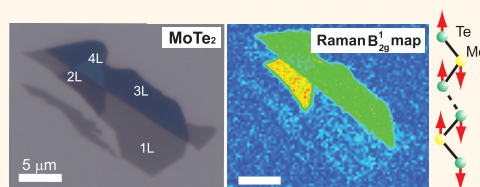
# Strong Enhancement of Raman Scattering from a Bulk-Inactive Vibrational Mode in Few-Layer MoTe<sub>2</sub>

Mahito Yamamoto,<sup>†,‡,\*</sup> Sheng Tsung Wang,<sup>‡,§,#</sup> Meiyang Ni,<sup>†,§,#</sup> Yen-Fu Lin,<sup>†,⊥</sup> Song-Lin Li,<sup>†</sup> Shinya Aikawa,<sup>†</sup> Wen-Bin Jian,<sup>‡</sup> Keiji Ueno,<sup>||</sup> Katsunori Wakabayashi,<sup>†</sup> and Kazuhito Tsukagoshi<sup>†,‡,\*</sup>

<sup>†</sup>International Center for Materials Nanoarchitectonics (WPI-MANA), National Institute for Materials Science (NIMS), Tsukuba, Ibaraki 305-0044, Japan, <sup>‡</sup>Department of Electrophysics, National Chiao Tung University, Hsinchu 30010, Taiwan, <sup>§</sup>School of Electronic Science and Applied Physics, Hefei University of Technology, Hefei 230009, China, <sup>⊥</sup>Department of Physics, National Chung Hsing University, Taichung, 40227, Taiwan, and <sup>||</sup>Department of Chemistry, Graduate School of Science and Engineering, Saitama University, Saitama 338-8570, Japan. <sup>#</sup>M. Yamamoto, S. T. Wang, and M. Ni contributed equally to this work.

**ABSTRACT** Two-dimensional layered crystals could show phonon properties that are markedly distinct from those of their bulk counterparts, because of the loss of periodicities along the *c*-axis directions. Here we investigate the phonon properties of bulk and atomically thin  $\alpha$ -MoTe<sub>2</sub> using Raman spectroscopy. The Raman spectrum of  $\alpha$ -MoTe<sub>2</sub> shows a prominent peak of the in-plane E<sub>2g</sub><sup>1</sup> mode, with its frequency upshifting with decreasing thickness down to the atomic scale, similar to other dichalcogenides.

Furthermore, we find large enhancement of the Raman scattering from the out-of-plane B<sub>2g</sub><sup>1</sup> mode in the atomically thin layers. The B<sub>2g</sub><sup>1</sup> mode is Raman inactive in the bulk, but is observed to become active in the few-layer films. The intensity ratio of the B<sub>2g</sub><sup>1</sup> to E<sub>2g</sub><sup>1</sup> peaks evolves significantly with decreasing thickness, in contrast with other dichalcogenides. Our observations point to strong effects of dimensionality on the phonon properties of MoTe<sub>2</sub>.



**KEYWORDS:** transition metal dichalcogenides · Raman spectroscopy · density functional theory · molybdenum ditelluride · MoS<sub>2</sub> · MoSe<sub>2</sub> · WSe<sub>2</sub>

Atomic layers of group VI transition metal dichalcogenides (MX<sub>2</sub>, where M = Mo and W and X = S, Se, and Te) have attracted much attention for a wide variety of applications ranging from spin- and valley-tronics to catalysts for hydrogen evolution reaction.<sup>1–5</sup> Of particular interest are their electronic and optoelectronic applications due to their large band gaps, together with the indirect-to-direct transitions in single-layers.<sup>6–10</sup> Field effect transistors with high on/off current ratios have been demonstrated using atomically thin MX<sub>2</sub>.<sup>11–14</sup> Single-layers of MoS<sub>2</sub> and WSe<sub>2</sub> have been used in optoelectronic devices including photodetectors and photoemitters.<sup>15–20</sup> Thanks to their large mechanical strength,<sup>21</sup> few-layers of MoS<sub>2</sub> and WS<sub>2</sub> have been used to fabricate flexible electronic devices.<sup>22–25</sup> Additionally, atomically thin MX<sub>2</sub> films have potential for thermoelectric applications, owing to their low thermal conductivities.<sup>26</sup>

A crucial step toward the application of atomically thin MX<sub>2</sub> is to understand its phonon properties. Phonons couple to electrons and limit carrier mobility at room

temperature,<sup>27,28</sup> along with Coulomb impurities.<sup>29,30</sup> Heat propagates in a crystal via predominantly acoustic phonons; thus, phonons determine its thermal conductivity.<sup>31,32</sup> Additionally, soft mode phonons determine the mechanical strength of the crystal.<sup>33</sup> Previously, Raman spectroscopy has been used to investigate the phonon properties of atomically thin MX<sub>2</sub>, including electron–phonon coupling<sup>34</sup> and the effects of heating<sup>35–37</sup> and strain<sup>38,39</sup> on the phonons. Moreover, Raman spectroscopy has shown that the lattice dynamics in MoS<sub>2</sub>, MoSe<sub>2</sub>, WS<sub>2</sub>, and WSe<sub>2</sub> depend sensitively on their thicknesses<sup>40–43</sup> and, hence, can be used to identify the number of layers at the atomic scale.

Here, we present, for the first time, Raman spectroscopy of atomically thin layers of  $\alpha$ -MoTe<sub>2</sub>. Bulk MoTe<sub>2</sub> is an indirect band gap semiconductor with a bandgap of 1.0 eV, but MoTe<sub>2</sub> is expected to exhibit a direct band gap of 1.1 eV in its single-layer,<sup>44–46</sup> similar to MoS<sub>2</sub>, MoSe<sub>2</sub>, WS<sub>2</sub>, and WSe<sub>2</sub>. Moreover, bulk MoTe<sub>2</sub> has been observed to undergo a transition from a diamagnetic

\* Address correspondence to yamamoto.mahito@nims.go.jp, kazuhito.tsukagoshi@nims.go.jp.

Received for review February 7, 2014 and accepted March 21, 2014.

Published online March 21, 2014  
10.1021/nn5007607

© 2014 American Chemical Society

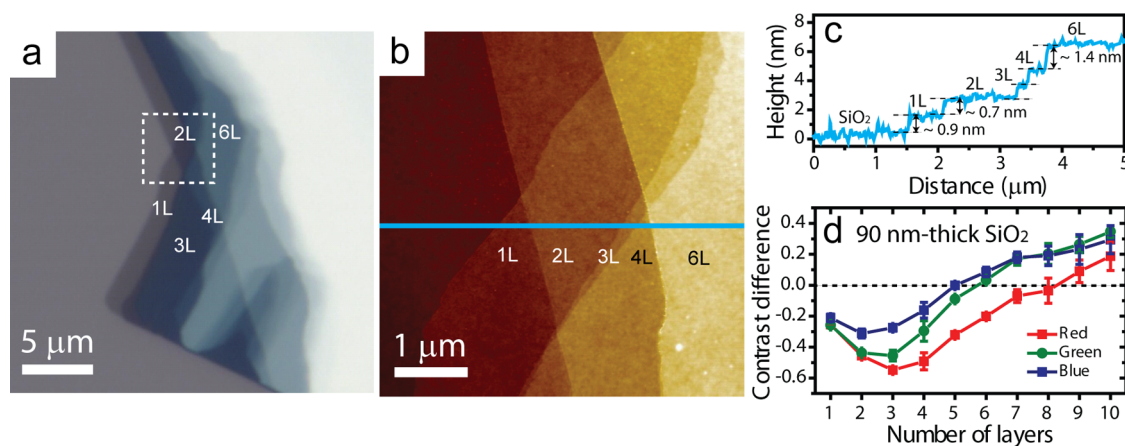


**Figure 1.** (a) Typical optical image of single- to multilayer MoTe<sub>2</sub> on 90 nm-thick SiO<sub>2</sub>. The number of layers (NL with  $N = 1-6$ ) is indicated. (b) An AFM image of the area surrounded by white dashed lines in (a). (c) A profile of the MoTe<sub>2</sub> flake along the blue line indicated in (b), showing a single-layer thickness of  $\sim 0.7$  nm between the layers. (d) Optical contrast differences between the MoTe<sub>2</sub> and SiO<sub>2</sub> surfaces for the red, green, and blue channels of the optical images, as functions of thickness. The contrast difference is normalized with the optical contrast of SiO<sub>2</sub> for each channel.

semiconducting  $\alpha$ -phase (trigonal prismatic) to a paramagnetic  $\beta$ -phase (distorted octahedral) at high temperatures,<sup>47,48</sup> offering unique potential for applications. However, though a few Raman spectroscopy studies of bulk MoTe<sub>2</sub> have been reported,<sup>49-51</sup> the lattice dynamics in atomically thin MoTe<sub>2</sub> has yet to be investigated.

The Raman spectrum of MoTe<sub>2</sub> shows a prominent peak of the in-plane  $E_{2g}^1$  mode at  $\sim 235$   $\text{cm}^{-1}$ , with a small out-of-plane  $A_{1g}$  peak at  $\sim 174$   $\text{cm}^{-1}$ . The  $E_{2g}^1$  mode upshifts, while the  $A_{1g}$  mode downshifts with decreasing thickness. Additionally, we find a strong peak at  $\sim 291$   $\text{cm}^{-1}$  in the atomically thin crystals. This peak is not observed in the bulk crystals, but the intensity is enhanced with decreasing thickness, down to bilayers. However, this peak is absent in single-layer MoTe<sub>2</sub>. We assign, using density functional theory (DFT) and group theory analysis, the peak as a bulk-Raman inactive mode of  $B_{2g}^1$ . The activation of the  $B_{2g}^1$  mode in atomically thin MoTe<sub>2</sub> is due to translation symmetry breaking along the  $c$ -axis direction. These findings suggest strong effects of symmetry breaking on the phonon properties of atomically thin MoTe<sub>2</sub>.

## RESULTS AND DISCUSSION

Bulk crystals of MoTe<sub>2</sub> were prepared through chemical vapor transport,<sup>52</sup> and were determined to have a  $2H_b$ -structure ( $\alpha$ -phase) by using X-ray photoelectron spectroscopy and X-ray diffraction.<sup>14</sup> Atomically thin MoTe<sub>2</sub> films were mechanically exfoliated from the bulk crystals onto silicon substrates with oxide layers on top. Figure 1a is a typical optical image of atomically thin MoTe<sub>2</sub> deposited on a 90 nm-thick SiO<sub>2</sub> substrate. We determine the thicknesses of the MoTe<sub>2</sub> films optically and using atomic force microscopy (AFM) in the tapping mode and Raman spectroscopy (see Figure S2 in Supporting Information for the identification of the number of layers from the Raman peak

intensity ratios).<sup>53</sup> Figure 1b is an AFM image of the area inside the white dashed lines indicated in Figure 1a. The profile along the blue line in Figure 1b shows a single layer spacing of  $\sim 0.7$  nm and a double layer spacing of  $\sim 1.4$  nm (Figure 1c). Hence, the thickness of the flake in the scanned area is identified to be a single-layer- to six-layers-thick (Figure 1a,b). The larger height of single-layer MoTe<sub>2</sub> shown in Figure 1c is due to either trapped contaminations at the MoTe<sub>2</sub>-SiO<sub>2</sub> interface, an artifact caused by the tapping mode AFM, or a combination of both.

We compare the optical contrasts between MoTe<sub>2</sub> of various thicknesses and the SiO<sub>2</sub> substrate to establish a reference for the identification of the number of layers. Figure 1d shows the optical contrast differences between the MoTe<sub>2</sub> and 90 nm-thick SiO<sub>2</sub> surfaces in gray scale for the red, green, and blue channels, as functions of the number of layers (the contrast difference is normalized with the contrast of the SiO<sub>2</sub> surface; see Methods and Section S3 in Supporting Information for details).<sup>54</sup> The contrast difference varies clearly with thickness up to 10 layers for each color channel and can be used to identify the thicknesses of the thin MoTe<sub>2</sub> films on SiO<sub>2</sub>, similar to other two-dimensional dichalcogenides (see Figures S3 and S4 in Supporting Information for the optical and the corresponding gray scale images of MoTe<sub>2</sub> with various thicknesses and the optical contrast differences between the MoTe<sub>2</sub> and 285 nm-thick SiO<sub>2</sub> surfaces).<sup>54-56</sup>

The  $\alpha$ -MoTe<sub>2</sub> crystal has a  $2H_b$ -MX<sub>2</sub> structure.<sup>47,52</sup> The  $2H_b$ -MX<sub>2</sub> crystal consists of layers of a trigonal prismatic X-M-X structure, as represented in Figure 2a. In the  $2H_b$  structure, the X-M-X layers are stacked in an AbABaB sequence, where the upper and lower cases represent X and M atoms. Therefore, bulk  $2H_b$ -MX<sub>2</sub> belongs to the  $D_{6h}^4$  symmetry group with M and X atoms in the  $D_{3h}$  and  $C_{3v}$  point groups, respectively. The irreducible representations of the phonons in bulk MX<sub>2</sub>

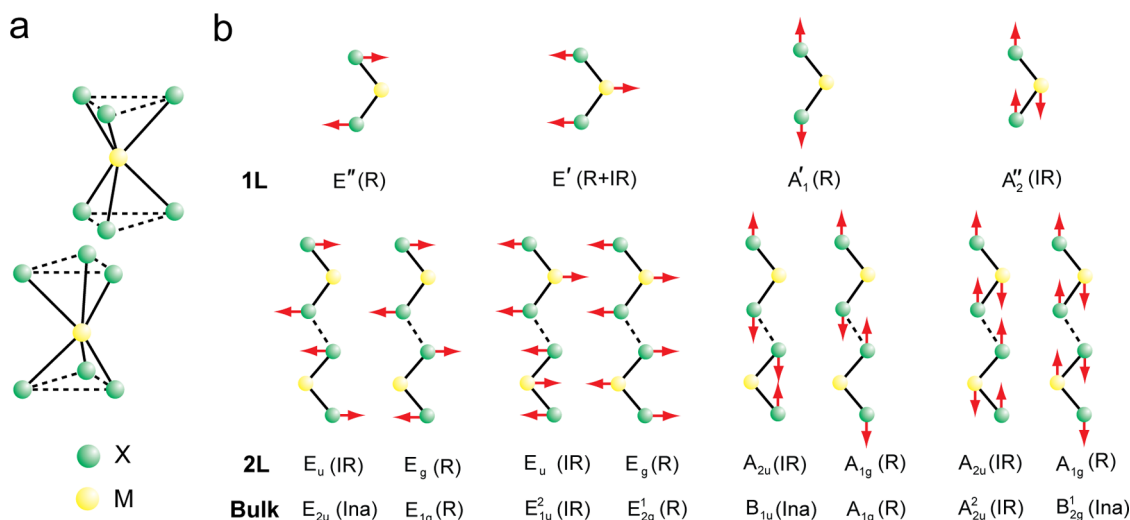


**Figure 2.** (a) Crystal structure of  $2H_b-MX_2$  in a repeat unit (two layers). The metal (M) and chalcogen (X) atoms are represented in yellow and green, respectively. (b) Phonon modes of single-layer (1L), bilayer (2L), and bulk  $2H_b-MX_2$  at the  $\Gamma$  point in the unit cell. Bilayer and bulk  $MX_2$  have phonon modes with equivalent atomic displacements, but different irreducible representations and optical activities. "R", "IR", and "Ina" indicate the Raman active, infrared active, and optically inactive modes. The black dashed lines connecting the X atoms indicate interlayer interactions.

at the Brillion zone center (the  $\Gamma$  point) are

$$\Gamma_{\text{bulk}} = A_{1g} + 2A_{2u} + 2B_{2g} + E_{1g} + 2E_{1u} + E_{2u} + B_{1u} + 2E_{2g} \quad (1)$$

where  $E_{1g}$ ,  $E^1_{2g}$ ,  $E^2_{2g}$ , and  $A_{1g}$  are Raman-active and  $E^1_{1u}$ ,  $E^2_{1u}$ ,  $A^1_{2u}$ , and  $A^2_{2u}$  are infrared active. The other modes are optically inactive. (Figure 2b; see also Figure S1 in Supporting Information for atomic displacements of all the  $\Gamma$  point phonon modes in bulk  $2H_b-MX_2$ ). Because of the loss of translation symmetry along the  $c$ -axis direction, single- and few-layers of  $2H_b-MX_2$  belong to different space groups, depending on the parity of the number of layers. Atomically thin crystals with an odd number of layers belong to the  $D^1_{3h}$  symmetry group without inversion symmetry, while crystals with an even number of layers belong to the  $D^3_{3d}$  symmetry group with inversion symmetry.<sup>57,58</sup> The irreducible representations of the  $\Gamma$  point phonons of the  $N$ -layer  $MX_2$  are thus

$$\Gamma_{\text{odd}} = \frac{3N-1}{2}(A'_1 + E'') + \frac{3N+1}{2}(A''_2 + E') \quad (2a)$$

for an odd number of  $N$  and

$$\Gamma_{\text{even}} = \frac{3N}{2}(A_{1g} + A_{2u} + E_g + E_u) \quad (2b)$$

for an even number of  $N$ , respectively.<sup>57,58</sup> Group theory predicts that the phonon modes in the single- and few-layer crystals exhibit different optical activities from those of the corresponding modes in the bulk. Among the phonon modes in single- and few-layer  $MX_2$ ,  $A'_1$ ,  $E''$ ,  $A_{1g}$ , and  $E_g$  are Raman active,  $A''_2$ ,  $A_{2u}$ , and  $E_u$  are infrared active, and  $E'$  is both Raman and infrared active. In Figure 2b, we find some phonon modes have equivalent atomic displacements but have different optical activities

for single- and bilayer and bulk  $MX_2$ . For example, the bulk-inactive  $E_{2u}$  mode becomes infrared active for bilayers ( $E_u$ ) and Raman active for a single-layer ( $E''$ ). Below, we denote the phonon modes of atomically thin crystals with the irreducible representations of the corresponding modes in the bulk, according to the literature. Raman spectroscopy of atomically thin  $2H_b-MoS_2$ ,  $MoSe_2$ ,  $WS_2$ , and  $WSe_2$  has shown peaks of the in-plane  $E^1_{2g}$  and out-of-plane  $A_{1g}$  modes.<sup>40-43</sup> Furthermore, peaks of an interlayer shear mode of  $E^2_{2g}$  have been observed at very low frequencies in few-layer  $MoS_2$  and  $WSe_2$ .<sup>57,59-61</sup> The  $E_{1g}$  mode is forbidden in the back-scattering configuration in the bulk, but has been detected in few-layers of  $WSe_2$ .<sup>58</sup>

We performed Raman spectroscopy of  $MoTe_2$ , using a solid-state laser with an excitation wavelength of 532 nm and a grating with 1800 grooves per millimeter, unless otherwise noted. Figure 3a shows the Raman spectra of single- to five- and 30-layer  $MoTe_2$ . The  $MoTe_2$  films show prominent peaks of the  $E^1_{2g}$  mode at  $\sim 235 \text{ cm}^{-1}$  and relatively weak peaks of the  $A_{1g}$  mode at  $\sim 174 \text{ cm}^{-1}$ , as previously observed in the bulk crystals.<sup>49-51</sup> The frequencies of these modes in  $MoTe_2$  are smaller than those observed in  $MoS_2$  and  $MoSe_2$  because of the larger weight of Te (see Section S4 in Supporting Information for the peak positions of the  $E^1_{2g}$  and  $A_{1g}$  modes in  $MoS_2$ ,  $MoSe_2$ , and  $MoTe_2$ ).<sup>8,40</sup> The peak near  $235 \text{ cm}^{-1}$  splits into two lines in 30-layer  $MoTe_2$ . While one of the peaks is the  $E^1_{2g}$  mode, another peak may be an infrared active mode of  $E^2_{1u}$  (the two modes are a conjugate pair with almost the same frequencies with a small shift induced by the interlayer interactions; see Figure 2b). The Raman activation of the  $E^2_{1u}$  mode has been reported in bulk  $MoS_2$  under the resonance condition,<sup>62,63</sup> but the cause of the activation

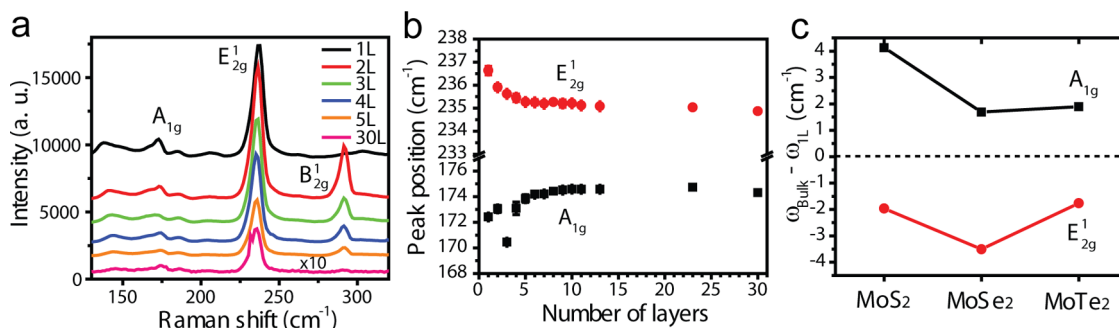


**Figure 3.** (a) Raman spectra of single- to five-layer and 30-layer MoTe<sub>2</sub>. The excitation wavelength is 532 nm. The Raman intensity of 30-layer MoTe<sub>2</sub> is magnified by 10 times. The peak at  $\sim 291$  cm<sup>-1</sup> in few-layer MoTe<sub>2</sub> is identified as the B<sup>1</sup><sub>2g</sub> mode in the text. (b) Peak positions of E<sup>1</sup><sub>2g</sub> (red circles) and A<sub>1g</sub> (black squares) for MoTe<sub>2</sub> as functions of the number of layers. (c) Frequency differences between the bulk and single-layer crystals,  $\omega_{\text{bulk}} - \omega_{1L}$ , for MoS<sub>2</sub>, MoSe<sub>2</sub>, and MoTe<sub>2</sub>. The red circles represent the E<sup>1</sup><sub>2g</sub> mode, and the black squares represent the A<sub>1g</sub> mode.

in MoTe<sub>2</sub> is unclear. We observe small peaks near 138 and 185 cm<sup>-1</sup>. These peaks may be the second-order Raman modes, as observed in other dichalcogenides.<sup>41–43</sup>

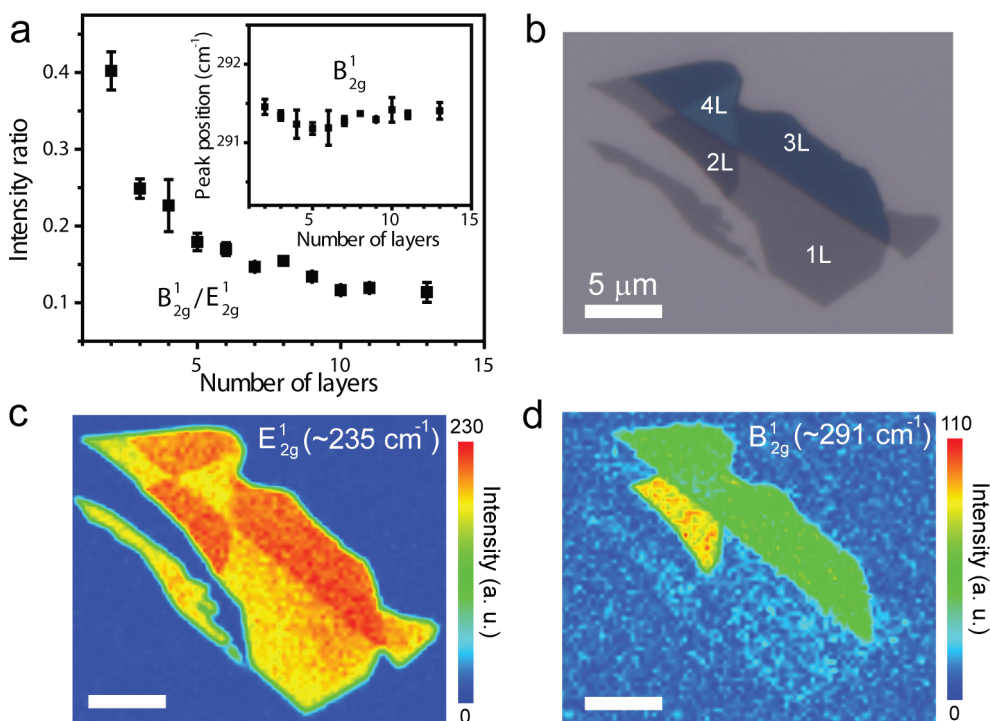
Figure 3b shows the peak positions of the E<sup>1</sup><sub>2g</sub> and A<sub>1g</sub> modes in MoTe<sub>2</sub> as functions of thickness. We find the E<sup>1</sup><sub>2g</sub> mode upshifts by  $\sim 1.5$  cm<sup>-1</sup>, while the A<sub>1g</sub> mode downshifts by  $\sim 2$  cm<sup>-1</sup>, with decreasing the number of layers from 30-layers to single-layer, as observed in other dichalcogenides.<sup>40–43</sup> The softening of the A<sub>1g</sub> mode in atomically thin layers is caused by the smaller effects of interlayer interactions that induce restoring forces to MoTe<sub>2</sub> molecules,<sup>40</sup> while the stiffening of the E<sup>1</sup><sub>2g</sub> mode may be due to effects of the boundary surface layers that lead to more effective forces to the MoTe<sub>2</sub> molecules with decreasing thickness.<sup>64</sup> We observe consistently an abrupt decrease in the A<sub>1g</sub> frequency at trilayer thickness. The A<sub>1g</sub> peak in trilayer MoTe<sub>2</sub> may be its “in-phase” vibrational mode, where the Te atoms in all three layers vibrate in phase (in the “out-of-phase” mode, the Te atoms in the middle layer vibrate 180° out-of-phase with respect to the outside layers). The “in-phase” and “out-of-phase” A<sub>1g</sub> modes in trilayer MoTe<sub>2</sub> are expected to have lower and higher frequencies, respectively, than the A<sub>1g</sub> mode of single-layer MoTe<sub>2</sub>, because of interlayer interactions.<sup>65</sup> However, we observe no clear peak of the “out-of-phase” A<sub>1g</sub> mode in trilayer MoTe<sub>2</sub>, likely because of the low spectral resolution of our Raman measurements. Further work using higher resolution Raman spectroscopy is needed to determine the cause of a decrease in the A<sub>1g</sub> frequency at trilayer thickness.

Figure 3c shows the frequency differences  $\omega_{\text{bulk}} - \omega_{1L}$  for MoS<sub>2</sub>, MoSe<sub>2</sub>, and MoTe<sub>2</sub>, where  $\omega_{\text{bulk}}$  and  $\omega_{1L}$  are the frequencies of the E<sup>1</sup><sub>2g</sub> and A<sub>1g</sub> modes of the bulk and single-layer crystals, respectively (see Section S4 in Supporting Information for the thickness-dependence of the E<sup>1</sup><sub>2g</sub> and A<sub>1g</sub> mode frequencies in MoS<sub>2</sub> and MoSe<sub>2</sub>). For the A<sub>1g</sub> mode, MoS<sub>2</sub> shows larger  $\omega_{\text{bulk}} - \omega_{1L}$  than MoSe<sub>2</sub> and MoTe<sub>2</sub>, while MoSe<sub>2</sub> and MoTe<sub>2</sub> show the small difference in  $\omega_{\text{bulk}} - \omega_{1L}$ . We also find no clear dependence of  $\omega_{\text{bulk}} - \omega_{1L}$  on compounds for the

E<sup>1</sup><sub>2g</sub> mode. These observations imply that the frequency difference between the bulk and single-layer crystals has a complex variation for the compounds, depending on the interlayer interactions, the molecular weights, and the surface effects.<sup>64</sup>

In addition to the E<sup>1</sup><sub>2g</sub> peak, we observe consistently a strong peak at  $\sim 291$  cm<sup>-1</sup> in atomically thin MoTe<sub>2</sub> (Figure 3a), which has been previously unassigned in Raman spectroscopy of bulk MoTe<sub>2</sub>.<sup>49–51</sup> This peak is also observed using a 633 nm excitation wavelength (see Figure S8 in Supporting Information for the Raman spectrum). Figure 4a plots the intensity ratio of the peak at  $\sim 291$  cm<sup>-1</sup> to the E<sup>1</sup><sub>2g</sub> peak as a function of thickness. The relative intensity is enhanced significantly with decreasing thickness and becomes the strongest in bilayer MoTe<sub>2</sub>. However, the peak is invariably absent in single-layer MoTe<sub>2</sub>, as shown in Figure 3a. The peak position has no clear thickness dependence (inset of Figure 4a). To investigate the spatial variation of the peak intensity, we perform Raman intensity mapping of atomically thin MoTe<sub>2</sub>. Figure 4c is a Raman intensity map of the E<sup>1</sup><sub>2g</sub> mode ( $\sim 235$  cm<sup>-1</sup>) of the single- to few-layer flake shown in Figure 4b. The Raman map shows a homogeneous intensity distribution over the surfaces of each layer, except at the edges, indicating that the crystal quality is spatially uniform. Raman intensity mapping of the peak at  $\sim 291$  cm<sup>-1</sup> on the same flake in Figure 4d shows no detectable intensity in the single-layer regions, but strong intensities are observed in the bilayer region. The intensity is reduced on tri- and four-layer surfaces. Similar to the E<sup>1</sup><sub>2g</sub> peak mapping, the peak intensity shows small spatial variations for each layer thickness.

These observations suggest that the phonon mode at  $\sim 291$  cm<sup>-1</sup> is Raman inactive in the bulk, but is intrinsically Raman-active in few-layer MoTe<sub>2</sub>, rather than activated externally, e.g., by defects or oxidation of MoTe<sub>2</sub>.<sup>62</sup> To identify the phonon mode of the peak at 291 cm<sup>-1</sup>, we calculate all of the phonon modes of  $\alpha$ -MoTe<sub>2</sub> at the  $\Gamma$  point for single- to trilayer and bulk



**Figure 4.** (a) Intensity ratio of the peak at  $\sim 291\text{ cm}^{-1}$  (which is identified to be the  $B_{2g}^1$  mode in the text) to the  $E_{2g}^1$  peak of  $\text{MoTe}_2$ , as a function of the number of layers. The inset is a plot of the peak position of the  $B_{2g}^1$  mode as a function of the number of layers. (b) An optical image of single- and few-layer  $\text{MoTe}_2$  on 90 nm-thick  $\text{SiO}_2$ . The number of layers (NL with  $N = 1$  to 4) is indicated. (b,c) Raman intensity maps of the  $\text{MoTe}_2$  films shown in (b) at frequencies of (c)  $\sim 235\text{ cm}^{-1}$  and (d)  $\sim 291\text{ cm}^{-1}$ . The background intensities are subtracted. The scale bars are  $5\ \mu\text{m}$ .

**TABLE 1. Calculated Frequencies (in  $\text{cm}^{-1}$ ) of the  $\Gamma$  Point Phonon Modes of Single-Layer (1L), Bilayer (2L), Trilayer (3L), and Bulk Crystals of  $\alpha\text{-MoTe}_2$ <sup>a</sup>**

	in-plane				out-of-plane			
1L	$E''$ (R) 120.2		$E'$ (R+IR) 242.3		$A_1'$ (R) 178.1		$A_2''$ (IR) 300.5	
2L	$E_u$ (IR) 119.8	$E_g$ (R) 121.0	$E_u$ (IR) 241.0	$E_g$ (R) 241.0	$A_{2u}$ (IR) 177.9	$A_{1g}$ (R) 180.2	$A_{2u}$ (IR) 297.7	$A_{1g}$ (R) 298.7
3L	$E''$ (R) 121.4		$E'$ (R+IR) 241.0		$A_1'$ (R) 179.4		$A_1'$ (R) 298.5	
	$E'$ (R+IR) 120.5		$E''$ (R) 241.0		$A_2''$ (IR) 178.3		$A_2''$ (IR) 298.2	
	$E''$ (R) 119.7		$E'$ (R+IR) 239.9		$A_1'$ (R) 177.0		$A_2''$ (IR) 295.9	
bulk	$E_{2u}$ (Ina) 119.3	$E_{1g}$ (R) 121.6	$E_{1u}^2$ (IR) 239.8	$E_{2g}^1$ (R) 239.9	$B_{1u}$ (Ina) 176.3	$A_{1g}$ (R) 179.9	$A_{2u}^2$ (IR) 290.4	$B_{2g}^1$ (Ina) 296.9

<sup>a</sup> Only high frequency phonons are shown. "R", "IR", and "Ina" indicate Raman- and infrared-active modes and optically inactive modes. The Raman/infrared activities of the phonon modes are determined from group theory.

crystals, by employing DFT. The DFT calculations were performed using the Vienna ab Simulation Package (VASP) within the local density approximation (LDA; see Methods for details).<sup>66,67</sup> Table 1 shows the calculated frequencies of the  $\Gamma$ -point phonon modes for single- to trilayer and bulk crystals of  $\alpha\text{-MoTe}_2$  with their Raman/infrared activities, determined by group theory (see Section S6 in Supporting Information for all the phonon frequencies calculated with DFT). The calculated frequencies of the  $E_{2g}^1$  and  $A_{1g}$  modes in bulk  $\text{MoTe}_2$  and the corresponding modes in single- and few-layer  $\text{MoTe}_2$  crystals are in reasonable agreement with the observed peak positions for each layer thickness, thus demonstrating the validity of the DFT calculations. In Table 1, we find no Raman-active

modes near  $291\text{ cm}^{-1}$  in single-layer and bulk  $\text{MoTe}_2$ , which is in consistent with the observations. The bi- and trilayer  $\text{MoTe}_2$  crystals both have Raman-active modes of  $A_{1g}$  and  $A_1'$  near the observed peak positions of  $291\text{ cm}^{-1}$ . Additionally, the Raman active  $A_{1g}$  mode is present near  $291\text{ cm}^{-1}$  in four-layer  $\text{MoTe}_2$  (see Table S2 in Supporting Information for the calculated frequencies of the phonon modes of four-layer  $\text{MoTe}_2$ ). Thus, we conclusively assign the observed peaks in few-layer  $\text{MoTe}_2$  at  $\sim 291\text{ cm}^{-1}$  as the out-of-plane vibrational modes of  $A_{1g}$  for an even number of layers and  $A_1'$  for an odd number of layers.

The  $A_{1g}$  and  $A_1'$  modes in few-layer crystals correspond to the  $B_{2g}^1$  mode in the bulk, which is optically inactive in  $2\text{H}_b\text{-MX}_2$  (see Figure 2 and Table 1).

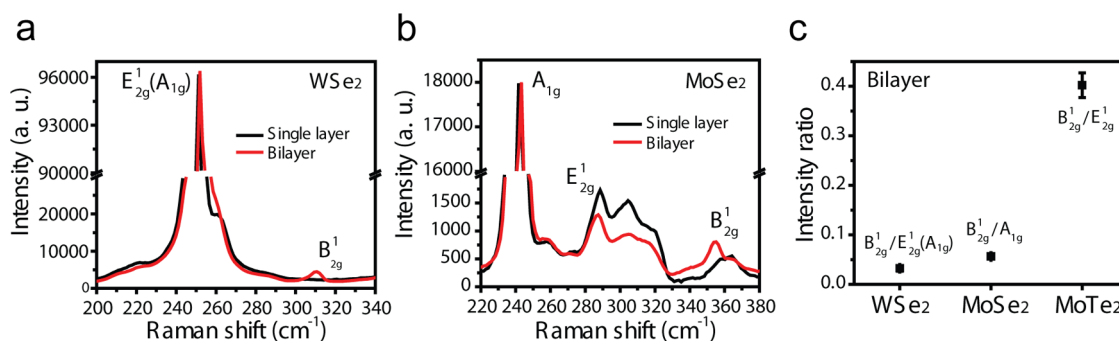


**Figure 5.** (a,b) Raman spectra of single-layer (black lines) and bilayers (red lines) of (a) WSe<sub>2</sub> and (b) MoSe<sub>2</sub>. The E<sub>2g</sub><sup>1</sup> peak intensities of the bilayer crystals are normalized with those of the single-layer crystals. (c) The intensity ratio of the B<sub>2g</sub><sup>1</sup> peak to each prominent peak (either E<sub>2g</sub><sup>1</sup> or A<sub>1g</sub>) of bilayer WSe<sub>2</sub>, MoSe<sub>2</sub>, and MoTe<sub>2</sub>.

A recent Raman spectroscopy study, along with DFT calculations and group theory analysis has reported that the B<sub>2g</sub><sup>1</sup> mode of WSe<sub>2</sub> becomes Raman active at the two-dimensional limit, because of translation symmetry breaking.<sup>58</sup> Furthermore, few-layer MoSe<sub>2</sub> has been observed to show a weak Raman peak possibly from the B<sub>2g</sub><sup>1</sup> mode.<sup>65</sup> Symmetry-breaking-induced Raman activation of a vibrational mode has also been observed in different groups of layered materials such as Bi<sub>2</sub>Te<sub>3</sub> and Bi<sub>2</sub>Se<sub>3</sub>.<sup>68–70</sup> The peak intensities of the symmetry-breaking-activated modes are reduced with increasing the number of layers because the crystals become more bulk-like with thickness. Indeed, we find the intensity ratio of the B<sub>2g</sub><sup>1</sup> peak to the E<sub>2g</sub><sup>1</sup> peak in MoTe<sub>2</sub> decreases with increasing thickness (Figure 4a). Accordingly, we determine crystal symmetry breaking along the *c*-axis direction as the cause of the Raman activation of the B<sub>2g</sub><sup>1</sup> mode in few-layer MoTe<sub>2</sub>. However, the B<sub>2g</sub><sup>1</sup> peak in atomically thin MoTe<sub>2</sub> is more strongly enhanced than in MoSe<sub>2</sub> and WSe<sub>2</sub>. Figure 5a,b are Raman spectra of single- and bilayer WSe<sub>2</sub> and MoSe<sub>2</sub> flakes that are mechanically cleaved from the bulk crystals onto 285 nm-thick SiO<sub>2</sub>. The WSe<sub>2</sub> and MoSe<sub>2</sub> bilayers show peaks of the B<sub>2g</sub><sup>1</sup> mode at ~310 and ~355 cm<sup>-1</sup>, which are absent in their single-layers. The intensities of the B<sub>2g</sub><sup>1</sup> peaks in WSe<sub>2</sub> and MoSe<sub>2</sub> are extremely weak, compared with those of their most prominent peaks of the E<sub>2g</sub><sup>1</sup> or A<sub>1g</sub> modes (the E<sub>2g</sub><sup>1</sup> and A<sub>1g</sub> modes are nearly degenerate in WSe<sub>2</sub> and, thus, they are indistinguishable experimentally in our Raman measurements). In Figure 5c, we show the intensity ratio of the B<sub>2g</sub><sup>1</sup> peak to each prominent peak of bilayer WSe<sub>2</sub>, MoSe<sub>2</sub>, and MoTe<sub>2</sub>. The relative intensities of the B<sub>2g</sub><sup>1</sup> peaks of WSe<sub>2</sub> and MoSe<sub>2</sub> are nearly 10 times smaller than that of MoTe<sub>2</sub>. The strong enhancement of the B<sub>2g</sub><sup>1</sup> peak intensity in atomically thin MoTe<sub>2</sub> is likely due to the large polarizability of the Te atom.<sup>50</sup> Additionally, the B<sub>2g</sub><sup>1</sup> peak is persistently observed in MoTe<sub>2</sub> with thicknesses ranging from two- to 13-layers, as shown in Figure 4a, but is diminished rapidly within several-layers in WSe<sub>2</sub> and MoSe<sub>2</sub>.<sup>58,65</sup> These results suggest strong effects of

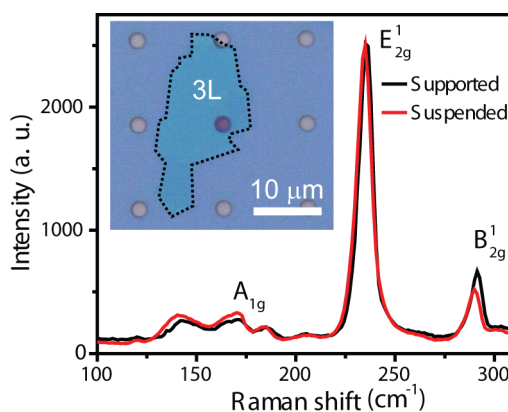


**Figure 6.** Raman spectra of trilayer (3L) MoTe<sub>2</sub> supported on SiO<sub>2</sub> (black line) and suspended over a hole (red line). The Raman spectrum of the suspended MoTe<sub>2</sub> flake is normalized with the E<sub>2g</sub><sup>1</sup> peak intensity of the supported MoTe<sub>2</sub> flake. The inset is an optical image of 3L MoTe<sub>2</sub> on 300 nm-thick SiO<sub>2</sub> with periodic arrays of holes with diameters of 2 μm. The edge of the MoTe<sub>2</sub> flake is highlighted by the black dashed lines.

dimensionality on the Raman activity of the B<sub>2g</sub><sup>1</sup> mode in MoTe<sub>2</sub>.

In addition to translation symmetry breaking, the optical activity of a vibrational mode in an atomically thin layered material might change due to coupling to an underlying substrate. Raman spectroscopy of atomically thin 2H<sub>b</sub>-TaSe<sub>2</sub> supported on SiO<sub>2</sub> shows a peak of the Raman E<sub>1g</sub> mode that is forbidden in the back-scattering geometry, but this peak is observed to be absent in free-standing TaSe<sub>2</sub>. The observations imply that interactions between TaSe<sub>2</sub> and SiO<sub>2</sub> lead to the Raman-activation of the E<sub>1g</sub> mode.<sup>71</sup> Lastly, we investigate the substrate effects on the Raman spectrum of atomically thin MoTe<sub>2</sub>. The atomically thin MoTe<sub>2</sub> films were exfoliated onto SiO<sub>2</sub> substrates that were pre-patterned with arrays of pits with diameters of 2–5 μm. The inset in Figure 6 is an optical image of trilayer MoTe<sub>2</sub> deposited on a SiO<sub>2</sub> substrate with pits with diameters of 2 μm. Figure 6 shows the Raman spectra of trilayer MoTe<sub>2</sub>, supported on SiO<sub>2</sub> and suspended over a pit. Both the supported- and suspended-MoTe<sub>2</sub> films show the B<sub>2g</sub><sup>1</sup> peaks with small differences in the

intensities, suggesting no obvious effect from the substrate on its Raman activation. Furthermore, we observe a small peak of the  $E_{1g}$  mode at  $\sim 120\text{ cm}^{-1}$  in both the supported- and suspended-MoTe<sub>2</sub> samples (see Figure S9 in Supporting Information for the expanded Raman spectra of MoTe<sub>2</sub> near  $\sim 120\text{ cm}^{-1}$ ). Thus, in contrast with TaSe<sub>2</sub>, the activation of the  $E_{1g}$  mode in trilayer MoTe<sub>2</sub> is due to crystal symmetry breaking rather than substrate effects, as previously observed in WSe<sub>2</sub>.<sup>58</sup> We find the suspended MoTe<sub>2</sub> films show lower Raman frequencies than the supported-MoTe<sub>2</sub> films. The redshift in the Raman peaks in the suspended films is due to the larger thermal effects induced by the incident laser, because of the lack of heat dissipation paths.<sup>35–37</sup>

## CONCLUSIONS

In summary, we have exfoliated atomically thin crystals of  $\alpha$ -MoTe<sub>2</sub> and investigated their thickness-dependent phonon properties with Raman spectroscopy. Similar to other dichalcogenides, the Raman  $E_{1g}^{1,2g}$  peak of MoTe<sub>2</sub> upshifts, while the  $A_{1g}$  peak downshifts,

with decreasing thickness down to the atomic scale. However, we have observed a strong peak in atomically thin MoTe<sub>2</sub>, which has been unassigned in bulk MoTe<sub>2</sub>. The peak intensity is enhanced largely with decreasing thickness, but the peak vanishes at single-layer thickness. We assign, by using group theory and DFT calculations within LDA, the observed peak as the bulk-Raman inactive  $B_{1,2g}^1$  mode. The activation of the  $B_{1,2g}^1$  peak at atomically thin thickness is due to translation symmetry breaking along the  $c$ -axis direction, rather than substrate effects. The relative peak intensity of the  $B_{1,2g}^1$  mode in atomically thin MoTe<sub>2</sub> is much stronger than those observed in WSe<sub>2</sub> and MoSe<sub>2</sub>. These observations suggest strong effects of symmetry breaking on the phonon properties of atomically thin MoTe<sub>2</sub>. In contrast to other dichalcogenides, very little is known about the electronic and optical properties of MoTe<sub>2</sub> in its atomically thin form. Our results could provide insight into the phonon properties of atomically thin MoTe<sub>2</sub> and also a strategy for identifying the number of layers of MoTe<sub>2</sub> at the atomic scale for further studies.

## METHODS

**Experimental Details.** Bulk crystals of  $\alpha$ -MoTe<sub>2</sub>, 2H<sub>b</sub>-MoSe<sub>2</sub>, and 2H<sub>b</sub>-WSe<sub>2</sub> were synthesized through chemical vapor transport.<sup>52</sup> For MoS<sub>2</sub>, commercially available crystals were used (Furuuchi Chemical Corporation). Atomically thin crystals of MoTe<sub>2</sub>, MoS<sub>2</sub>, MoSe<sub>2</sub>, and WSe<sub>2</sub> were exfoliated mechanically from the bulk crystals onto SiO<sub>2</sub> with a thickness of either 90 or 285 nm, using adhesive tape. To obtain the suspended MoTe<sub>2</sub> samples, atomically thin MoTe<sub>2</sub> films were deposited onto 300 nm-thick SiO<sub>2</sub> substrates that were prepatterned with periodic arrays of pits with diameters ranging from 2 to 5  $\mu\text{m}$ . The patterns were fabricated using photolithography and dry etching processes. The thicknesses of the atomically thin crystals were identified optically and with Raman spectroscopy and atomic force microscopy.<sup>40,43,53</sup> For the optical contrast analysis, gray scale images were extracted from the bare optical images for the red, green, and blue components by using ImageJ.<sup>54</sup> Raman spectroscopy was performed in the backscattering configuration using 532 and 633 nm excitation lasers, a 100 $\times$  objective, and a grating with 1800 grooves/mm (Tokyo Instruments, Inc.). The laser power was kept below 0.1 mW to avoid any damage to the samples. Atomic force microscopy was performed at room temperature in the tapping mode with silicon cantilevers (Seiko Instruments Inc.).

**Calculation Details.** Density functional theory calculations were performed using the Vienna ab Simulation Package.<sup>66,67</sup> The core and valence electrons in the atoms were described with the projector-augmented wave method. The exchange-correlation functional was treated with the local density approximation, which gives a good description of the geometrical and phonon properties of layered materials. The plane-wave basis set cutoff was 500 eV for MoTe<sub>2</sub>. Monkhorst-Pack  $k$ -point meshes of  $9 \times 9 \times 1$  and  $9 \times 9 \times 5$  were used for the thin films and the bulk, respectively. To avoid interactions between the periodic images of the thin films in the stacking direction, a vacuum thickness of 15 Å was used. All of the structures were completely optimized with convergence thresholds of  $10^{-6}$  eV for the energies and  $10^{-3}$  eV/Å for the forces. The phonon frequencies and eigenvectors were calculated using density functional perturbation theory.

**Conflict of Interest:** The authors declare no competing financial interest.

**Acknowledgment.** We thank Yasushi Morihira and Hiroyuki Watabe from Tokyo Instruments, Inc., for their technical support

in the Raman measurement. This research was supported by a Grant-in-Aid (Kakenhi No. 25107004) from the Japan Society for the Promotion of Science (JSPS) through the Funding Program for World-Leading Innovative R&D on Science and Technology (FIRST), initiated by the Council for Science and Technology Policy (CSTP) of Japan, and Experiment-Theory Fusion trial project by MANA.

**Supporting Information Available:** The  $\Gamma$ -point phonon modes of bulk 2H<sub>b</sub>-MX<sub>2</sub>, identification of the number of layers of MoTe<sub>2</sub> from the Raman intensity ratios, optical contrast differences between atomically thin MoTe<sub>2</sub> and SiO<sub>2</sub> surfaces, peak positions and intensities of the  $E_{1,2g}^1$  and  $A_{1g}$  modes and their thickness-dependences for MoS<sub>2</sub>, MoSe<sub>2</sub>, and MoTe<sub>2</sub>, the 633 nm-excited Raman spectrum of atomically thin MoTe<sub>2</sub>, the calculated phonon frequencies of MoTe<sub>2</sub>, and Raman spectra of supported- and suspended-MoTe<sub>2</sub>. This material is available free of charge via the Internet at <http://pubs.acs.org>.

## REFERENCES AND NOTES

- Wang, Q. H.; Kalantar-Zadeh, K.; Kis, A.; Coleman, J. N.; Strano, M. S. Electronics and Optoelectronics of Two-Dimensional Transition Metal Dichalcogenides. *Nat. Nanotechnol.* **2012**, *7*, 699–712.
- Chhowalla, M.; Shin, H. S.; Eda, G.; Li, L. -J.; Loh, K. P.; Zhang, H. The Chemistry of Two-Dimensional Layered Transition Metal Dichalcogenide Nanosheets. *Nat. Chem.* **2013**, *5*, 263–275.
- Butler, S. Z.; Hollen, S. M.; Cao, L.; Cui, Y.; Gupta, J. A.; Gutiérrez, H. R.; Heinz, T. F.; Hong, S. S.; Huang, J.; Ismach, A. F.; *et al.* Progress, Challenges, and Opportunities in Two-Dimensional Materials Beyond Graphene. *ACS Nano* **2013**, *7*, 2898–2926.
- Xu, M.; Liang, T.; Shi, M.; Chen, H. Graphene-like Two-Dimensional Materials. *Chem. Rev.* **2013**, *113*, 3766–3798.
- Song, X.; Hu, J.; Zeng, H. Two-Dimensional Semiconductors: Recent Progress and Future Perspectives. *J. Mater. Chem. C* **2013**, *1*, 2952–2969.
- Mak, K. F.; Lee, C.; Hone, J.; Shan, J.; Heinz, T. F. Atomically Thin MoS<sub>2</sub>: A New Direct-Gap Semiconductor. *Phys. Rev. Lett.* **2010**, *105*, 136805.
- Splendiani, A.; Sun, L.; Zhang, Y.; Li, T.; Kim, J.; Chim, C. -Y.; Galli, G.; Wang, F. Emerging Photoluminescence in Monolayer MoS<sub>2</sub>. *Nano Lett.* **2010**, *10*, 1271–1275.

8. Tongay, S.; Zhou, J.; Ataca, C.; Lo, K.; Matthews, T. S.; Li, J.; Grossman, J. C.; Wu, J. Thermally Driven Crossover from Indirect Toward Direct Bandgap in 2D Semiconductors: MoSe<sub>2</sub> versus MoS<sub>2</sub>. *Nano Lett.* **2012**, *12*, 5576–5580.
9. Gutiérrez, H. R.; Perea-López, N.; Elías, A. L.; Berkdemir, A.; Wang, B.; Lv, R.; López-Urías, F.; Crespi, V. H.; Terrones, H.; Terrones, M. Extraordinary Room-Temperature Photoluminescence in Triangular WS<sub>2</sub> Monolayers. *Nano Lett.* **2013**, *13*, 3447–3454.
10. Zhao, W.; Ghorannevis, Z.; Chu, L.; Toh, M.; Kloc, C.; Tan, P. -H.; Eda, G. Evolution of Electronic Structure in Atomically Thin Sheets of WS<sub>2</sub> and WSe<sub>2</sub>. *ACS Nano* **2013**, *7*, 791–797.
11. Radisavljevic, B.; Radenovic, A.; Brivio, J.; Giacometti, V.; Kis, A. Single-Layer MoS<sub>2</sub> Transistors. *Nat. Nanotechnol.* **2011**, *6*, 147–150.
12. Fang, H.; Chuang, S.; Chang, T. C.; Takei, K.; Takahashi, T.; Javey, A. High-Performance Single Layered WSe<sub>2</sub> p-FETs with Chemically Doped Contacts. *Nano Lett.* **2012**, *12*, 3788–3792.
13. Larentis, S.; Fallahazad, B.; Tutuc, E. Field-Effect Transistors and Intrinsic Mobility in Ultra-Thin MoSe<sub>2</sub> Layers. *Appl. Phys. Lett.* **2012**, *101*, 223104.
14. Lin, Y. -F.; Xu, Y.; Wang, S. -T.; Li, S. -L.; Yamamoto, M.; Aparecido-Ferreira, A.; Li, W.; Sun, H.; Nakaharai, S.; Jian, W. -B.; et al. Ambipolar MoTe<sub>2</sub> Transistors and Their Applications in Logic Circuits. *Adv. Mater.*, accepted.
15. Yin, Z.; Li, H.; Li, H.; Jiang, L.; Shi, Y.; Sun, Y.; Lu, G.; Zhang, Q.; Chen, X.; Zhang, H. Single-Layer MoS<sub>2</sub> Phototransistors. *ACS Nano* **2012**, *6*, 74–80.
16. Lopez-Sanchez, O.; Lembke, D.; Kayci, M.; Radenovic, A.; Kis, A. Ultrasensitive Photodetectors Based on Monolayer MoS<sub>2</sub>. *Nat. Nanotechnol.* **2013**, *8*, 497–501.
17. Sundaram, R. S.; Engel, M.; Lombardo, A.; Krupke, R.; Ferrari, A. C.; Avouris, P.; Steiner, M. Electroluminescence in Single Layer MoS<sub>2</sub>. *Nano Lett.* **2013**, *13*, 1416–1421.
18. Baugher, B. W. H.; Churchill, H. O. H.; Yang, Y.; Jarillo-Herrero, P. Optoelectronic Devices Based on Electrically Tunable p–n Diodes in a Monolayer Dichalcogenide. *Nat. Nanotechnol.* **2014**, 10.1038/nnano.2014.25.
19. Ross, J. S.; Klement, P.; Jones, A. M.; Ghimire, N. J.; Yan, J.; Mandrus, D. G.; Taniguchi, T.; Watanabe, K.; Kitamura, K.; Yao, W.; et al. Electrically Tunable Excitonic Light-Emitting Diodes Based on Monolayer WSe<sub>2</sub> p–n Junctions. *Nat. Nanotechnol.* **2014**, 10.1038/nnano.2014.26.
20. Pospischil, A.; Furchi, M. M.; Mueller, T. Solar-Energy Conversion and Light Emission in an Atomic Monolayer p–n Diode. *Nat. Nanotechnol.* **2014**, 10.1038/nnano.2014.14.
21. Bertolazzi, S.; Brivio, J.; Kis, A. Stretching and Breaking of Ultrathin MoS<sub>2</sub>. *ACS Nano* **2011**, *12*, 9703–9709.
22. Pu, J.; Yomogida, Y.; Liu, K. -K.; Li, L. -J.; Iwasa, Y.; Takenobu, T. Highly Flexible MoS<sub>2</sub> Thin-Film Transistors with Ion Gel Dielectrics. *Nano Lett.* **2012**, *12*, 4013–4017.
23. Salvatore, G. A.; Münzrieder, N.; Barraud, C.; Petti, L.; Zysset, C.; Büthe, L.; Ensslin, K.; Tröster, G. Fabrication and Transfer of Flexible Few-Layers MoS<sub>2</sub> Thin Film Transistors to Any Arbitrary Substrate. *ACS Nano* **2013**, *7*, 8809–8815.
24. Lee, G. -H.; Yu, Y. -J.; Cui, X.; Petrone, N.; Lee, C. -H.; Choi, M. S.; Lee, D. -Y.; Lee, C.; Yoo, W. J.; Watanabe, K.; et al. Flexible and Transparent MoS<sub>2</sub> Field-Effect Transistors on Hexagonal Boron Nitride-Graphene Heterostructures. *ACS Nano* **2013**, *7*, 7931–7936.
25. Yu, W. J.; Li, Z.; Zhou, H.; Chen, Y.; Wang, Y.; Huang, Y.; Duan, X. Vertically Stacked Multi-Heterostructures of Layered Materials for Logic Transistors and Complementary Inverters. *Nat. Mater.* **2013**, *12*, 246–252.
26. Huang, W.; Da, H.; Liang, G. Thermoelectric Performance of MX<sub>2</sub> (M = Mo, W; X = S, Se) Monolayers. *J. Appl. Phys.* **2013**, *113*, 104304.
27. Kaasbjerg, K.; Thygesen, K. S.; Jacobsen, K. W. Phonon-Limited Mobility in n-Type Single-Layer MoS<sub>2</sub> from First Principles. *Phys. Rev. B: Condens. Matter Mater. Phys.* **2012**, *85*, 115317.
28. Kaasbjerg, K.; Thygesen, K. S.; Jauho, A. -P. Acoustic Phonon Limited Mobility in Two-Dimensional Semiconductors: Deformation Potential and Piezoelectric Scattering in Monolayer MoS<sub>2</sub> from First Principles. *Phys. Rev. B: Condens. Matter Mater. Phys.* **2013**, *87*, 235312.
29. Ghatak, S.; Pal, A. N.; Ghosh, A. Nature of Electronic States in Atomically Thin MoS<sub>2</sub> Field-Effect Transistors. *ACS Nano* **2011**, *5*, 7707–7712.
30. Li, S. -L.; Wakabayashi, K.; Xu, Y.; Nakaharai, S.; Komatsu, K.; Li, W. -W.; Lin, Y. -F.; Aparecido-Ferreira, A.; Tsukagoshi, K. Thickness-Dependent Interfacial Coulomb Scattering in Atomically Thin Field-Effect Transistors. *Nano Lett.* **2013**, *13*, 3546–3552.
31. Liu, X.; Zhang, G.; Pei, Q. -X.; Zhang, Y. -W. Phonon Thermal Conductivity of Monolayer MoS<sub>2</sub> Sheet and Nanoribbons. *Appl. Phys. Lett.* **2013**, *103*, 133113.
32. Li, W.; Carrete, J.; Mingo, N. Thermal Conductivity and Phonon Linewidths of Monolayer MoS<sub>2</sub> from First Principles. *Appl. Phys. Lett.* **2013**, *103*, 253103.
33. Li, T. Ideal Strength and Phonon Instability in Single-Layer MoS<sub>2</sub>. *Phys. Rev. B: Condens. Matter Mater. Phys.* **2012**, *85*, 235407.
34. Chakraborty, B.; Bera, A.; Muthu, D. V. S.; Bhowmick, S.; Waghmare, U. V.; Sood, A. K. Symmetry-Dependent Phonon Renormalization in Monolayer MoS<sub>2</sub> Transistor. *Phys. Rev. B: Condens. Matter Mater. Phys.* **2012**, *85*, 161403(R).
35. Najmaei, S.; Liu, Z.; Ajayan, P. M.; Lou, J. Thermal Effects on the Characteristic Raman Spectrum of Molybdenum Disulfide (MoS<sub>2</sub>) of Varying Thicknesses. *Appl. Phys. Lett.* **2012**, *100*, 013106.
36. Sahoo, S.; Gaur, A. P. S.; Ahmadi, M.; Guinel, M. J. -F.; Katiyar, R. S. Temperature-Dependent Raman Studies and Thermal Conductivity of Few-Layer MoS<sub>2</sub>. *J. Phys. Chem. C* **2013**, *117*, 9042–9047.
37. Yan, R.; Simpson, J. R.; Bertolazzi, S.; Brivio, J.; Watson, M.; Wu, X.; Kis, A.; Luo, T.; Walker, A. R. H.; King, H. G. Thermal Conductivity of Monolayer Molybdenum Disulfide Obtained from Temperature-Dependent Raman Spectroscopy. *ACS Nano* **2014**, *8*, 986–993.
38. Rice, C.; Young, R. J.; Zan, R.; Bangert, U.; Wolverson, D.; Georgiou, T.; Jalil, R.; Novoselov, K. S. Raman-Scattering Measurements and First-Principles Calculations of Strain-Induced Phonon Shifts in Monolayer MoS<sub>2</sub>. *Phys. Rev. B: Condens. Matter Mater. Phys.* **2013**, *87*, 081307(R).
39. Wang, Y.; Cong, C.; Qiu, C.; Yu, T. Raman Spectroscopy Study of Lattice Vibration and Crystallographic Orientation of Monolayer MoS<sub>2</sub> under Uniaxial Strain. *Small* **2013**, *9*, 2857–2861.
40. Lee, C.; Yan, H.; Brus, L. E.; Heinz, T. F.; Hone, J.; Ryu, S. Anomalous Lattice Vibrations of Single- and Few-Layer MoS<sub>2</sub>. *ACS Nano* **2010**, *4*, 2695–2700.
41. Li, H.; Zhang, Q.; Yap, C. C. R.; Tay, B. K.; Edwin, T. H. T.; Olivier, A.; Baillargeat, D. From Bulk to Monolayer MoS<sub>2</sub>: Evolution of Raman Scattering. *Adv. Funct. Mater.* **2012**, *22*, 1385–1390.
42. Berkdemir, A.; Gutiérrez, H. R.; Botello-Méndez, A. R.; Perea-López, N.; Elías, A. L.; Chia, C. -I.; Wang, B.; Crespi, V. H.; López-Urías, F.; Charlier, J. -C.; et al. Identification of Individual and Few Layers of WS<sub>2</sub> Using Raman Spectroscopy. *Sci. Rep.* **2013**, *3*, 1755.
43. Zhao, W.; Ghorannevis, Z.; Amara, K. K.; Pang, J. R.; Toh, M.; Zhang, X.; Kloc, C.; Tan, P. H.; Eda, G. Lattice Dynamics in Mono- and Few-Layer Sheets of WS<sub>2</sub> and WSe<sub>2</sub>. *Nanoscale* **2013**, *5*, 9677–9683.
44. Ding, Y.; Wang, Y.; Ni, J.; Shi, L.; Shi, S.; Tang, W. First Principles Study of Structural, Vibrational and Electronic Properties of Graphene-like MX<sub>2</sub> (M = Mo, Nb, W, Ta; X = S, Se, Te) Monolayers. *Physica B* **2011**, *406*, 2254–2260.
45. Ataca, C.; Şahin, H.; Ciraci, S. Stable, Single-Layer MX<sub>2</sub> Transition-Metal Oxides and Dichalcogenides in a Honeycomb-like Structure. *J. Phys. Chem. C* **2012**, *116*, 8983–8999.
46. Ma, Y.; Dai, Y.; Guo, M.; Niu, C.; Lu, J.; Huang, B. Electronic and Magnetic Properties of Perfect, Vacancy-Doped, and Nonmetal Adsorbed MoSe<sub>2</sub>, MoTe<sub>2</sub> and WS<sub>2</sub> Monolayers. *Phys. Chem. Chem. Phys.* **2011**, *13*, 15546–15553.
47. Vellinga, M. B.; de Jonge, R.; Haas, C. Semiconductor to Metal Transition in MoTe<sub>2</sub>. *J. Solid State Chem.* **1970**, *2*, 299–302.
48. Dawson, W. G.; Bullett, D. W. Electronic Structure and Crystallography of MoTe<sub>2</sub> and WTe<sub>2</sub>. *J. Phys. C: Solid State Phys.* **1987**, *20*, 6159–6174.



49. Wieting, T. J.; Grisel, A.; Lévy, F. Interlayer Bonding and Localized Charge in  $\text{MoSe}_2$  and  $\alpha\text{-MoTe}_2$ . *Physica B* **1980**, *99*, 337–342.
50. Sugai, S.; Ueda, T. High-Pressure Raman Spectroscopy in the Layered Materials  $2\text{H-MoS}_2$ ,  $2\text{H-MoSe}_2$ , and  $2\text{H-MoTe}_2$ . *Phys. Rev. B: Condens. Matter Mater. Phys.* **1982**, *26*, 6554–6558.
51. Agnihotri, O. P.; Sehgal, H. K.; Garg, A. K. Laser Excited Raman Spectra of Gr. VI Semiconducting Compounds. *Solid State Commun.* **1973**, *12*, 135–138.
52. Lieth, R. M. A. *Preparation and Crystal Growth of Materials with Layered Structures*; Springer: Berlin, 1977; Vol. 1.
53. Li, S. -L.; Miyazaki, H.; Song, H.; Kuramochi, H.; Nakaharai, S.; Tsukagoshi, K. Quantitative Raman Spectrum and Reliable Thickness Identification for Atomic Layers on Insulating Substrates. *ACS Nano* **2012**, *6*, 7381–7388.
54. Li, H.; Wu, J.; Huang, X.; Lu, G.; Yang, J.; Lu, X.; Xiong, Q.; Zhang, H. Rapid and Reliable Thickness Identification of Two-Dimensional Nanosheets Using Optical Microscopy. *ACS Nano* **2013**, *7*, 10344–10353.
55. Castellanos-Gomez, A.; Agrait, N.; Rubio-Bollinger, G. Optical Identification of Atomically Thin Dichalcogenide Crystals. *Appl. Phys. Lett.* **2010**, *96*, 213116.
56. Castellanos-Gomez, A.; Navarro-Moratalla, E.; Mokry, G.; Quereda, J.; Pinilla-Cienfuegos, E.; Agrait, N.; van der Zant, H. S. J.; Coronado, E.; Steele, G. A.; Rubio-Bollinger, G. Fast and Reliable Identification of Atomically Thin Layers of  $\text{TaSe}_2$  Crystals. *Nano Res.* **2013**, *6*, 191–199.
57. Zhao, Y.; Luo, X.; Li, H.; Zhang, J.; Araujo, P. T.; Gan, C. K.; Wu, J.; Zhang, H.; Quek, S. Y.; Dresselhaus, M. S.; *et al.* Interlayer Breathing and Shear Modes in Few-Trilayer  $\text{MoS}_2$  and  $\text{WSe}_2$ . *Nano Lett.* **2013**, *13*, 1007–1015.
58. Luo, X.; Zhao, Y.; Zhang, J.; Toh, M.; Kloc, C.; Xiong, Q.; Quek, S. Y. Effects of Lower Symmetry and Dimensionality on Raman Spectra in Two-Dimensional  $\text{WSe}_2$ . *Phys. Rev. B: Condens. Matter Mater. Phys.* **2013**, *88*, 195313.
59. Plechinger, G.; Heydrich, S.; Eroms, J.; Weiss, D.; Schüller, C.; Korn, T. Raman Spectroscopy of the Interlayer Shear Mode in Few-Layer  $\text{MoS}_2$  Flakes. *Appl. Phys. Lett.* **2012**, *101*, 101906.
60. Zeng, H.; Zhu, B.; Liu, K.; Fan, J.; Cui, X.; Zhang, Q. M. Low-Frequency Raman Modes and Electronic Excitations in Atomically Thin  $\text{MoS}_2$  Films. *Phys. Rev. B: Condens. Matter Mater. Phys.* **2012**, *86*, 241301(R).
61. Zhang, X.; Han, W. P.; Wu, J. B.; Milana, S.; Lu, Y.; Li, Q. Q.; Ferrari, A. C.; Tan, P. H. Raman Spectroscopy of Shear and Layer Breathing Modes in Multilayer  $\text{MoS}_2$ . *Phys. Rev. B: Condens. Matter Mater. Phys.* **2013**, *87*, 115413.
62. Windom, B. C.; Sawyer, W. G.; Hahn, D. W. A Raman Spectroscopic Study of  $\text{MoS}_2$  and  $\text{MoO}_3$ : Applications to Tribological Systems. *Tribol. Lett.* **2011**, *42*, 301–310.
63. Sekine, T.; Uchinokura, K.; Nakashizu, T.; Matsuura, E.; Yoshizaki, R. Dispersive Raman Mode of Layered Compound  $2\text{H-MoS}_2$  under Resonant Condition. *J. Phys. Soc. Jpn.* **1984**, *53*, 811–818.
64. Luo, X.; Zhao, Y.; Zhang, J.; Xiong, Q.; Quek, S. Y. Anomalous Frequency Trends in  $\text{MoS}_2$  Thin Films Attributed to Surface Effects. *Phys. Rev. B: Condens. Matter Mater. Phys.* **2013**, *88*, 075320.
65. Tonndorf, P.; Schmidt, R.; Böttger, P.; Zhang, X.; Börner, J.; Liebig, A.; Albrecht, M.; Kloc, C.; Gordan, O.; Zahn, D. R. T.; *et al.* Photoluminescence Emission and Raman Response of Monolayer  $\text{MoS}_2$ ,  $\text{MoSe}_2$ , and  $\text{WSe}_2$ . *Opt. Express* **2013**, *21*, 4908–4916.
66. Kresse, G.; Furthmüller, J. Efficiency of *Ab-Initio* Total Energy Calculations for Metals and Semiconductors Using a Plane-Wave Basis Set. *Comput. Mater. Sci.* **1996**, *6*, 15–50.
67. Kresse, G.; Furthmüller, J. Efficient Iterative Schemes for *Ab Initio* Total-Energy Calculations Using a Plane-Wave Basis Set. *Phys. Rev. B: Condens. Matter Mater. Phys.* **1996**, *54*, 11169–11186.
68. Shahil, K. M. F.; Hossain, M. Z.; Teweldebrhan, D.; Balandin, A. A. Crystal Symmetry Breaking in Few-Quintuple  $\text{Bi}_2\text{Te}_3$  Films: Applications in Nanometrology of Topological Insulators. *Appl. Phys. Lett.* **2010**, *96*, 153103.
69. Teweldebrhan, D.; Goyal, V.; Balandin, A. A. Exfoliation and Characterization of Bismuth Telluride Atomic Quintuples and Quasi-Two-Dimensional Crystals. *Nano Lett.* **2010**, *10*, 1209–1218.
70. Shahil, K. M. F.; Hossain, M. Z.; Goyal, V.; Balandin, A. A. Micro-Raman Spectroscopy of Mechanically Exfoliated Few-Quintuple Layers of  $\text{Bi}_2\text{Te}_3$ ,  $\text{Bi}_2\text{Se}_3$ , and  $\text{Sb}_2\text{Te}_3$  Materials. *J. Appl. Phys.* **2012**, *111*, 054305.
71. Hajiyev, P.; Cong, C.; Qiu, C.; Yu, T. Contrast and Raman Spectroscopy Study of Single- and Few-Layered Charge Density Wave Material:  $2\text{H-TaSe}_2$ . *Sci. Rep.* **2013**, *3*, 2593.